Evaluation and Validation of the Net Primary Productivity of the Zoigê Wetland Based on Grazing Coupled Remote Sensing Process Model

Li He, Chengying Li, Zhengwei He, Xian Liu, and Rui Qu

***Abstract*—Zoigê wetland is located in the southeastern edge of the Qinghai–Tibet Plateau, in recent years, the wetland local area grassland productivity decline, land sanding, and other serious degradation phenomenon. Using remote sensing and hydrology data combined with the basic principles of vegetation ecology, we applied the Carnegie–Ames–Stanford Approach (CASA) model and Boreal Ecosystem Productivity Simulator (BEPS) model to invert the net primary productivity (NPP) of the Zoigê wetland ecosystem and then identified the deficiencies of the two models. In this article, we tested the factors that influence the light use efficiency of vegetation and considered the effects of livestock grazing on grassland ecosystems and wetland moisture content on vegetation growth. A new grazing coupled remote sensing process (GCRSP) model suitable for the productivity of the Zoigê wetland was proposed. Field survey data were combined with the CASA model, BEPS model, and Moderate Resolution Imaging Spectroradiometer (MODIS) NPP product, and the accuracy of the proposed GCRSP model was analyzed at regional level. The results show that after fitting the field measurements to the GCRSP model, the fitted variance between the model and the measured data is 0.84, which is larger than the variance between the other two methods and the measured data. In addition, the variance of the linear fit between the GCRSP model and the MODIS NPP product was 0.11, which was relatively small, indicating that the regional-scale GCRSP model was relatively accurate for the Zoigê wetland NPP. Therefore, this model was suitable for the inversion of regional-scale NPP. The results indicated that the average grassland NPP of the Zoigê wetland was 487.57 gC/m^2, and larger NPP values were distributed near the rivers and wetland and smaller NPP values were distributed in the mountain glacier and desertified land areas. These results were consistent with the regional characteristics. This article provided technical and theoretical support for the desertification management of the Zoigê grassland and a new method for studying vegetation NPP, and the findings could help improve the accuracy of regional-scale vegetation NPP estimates.**

***Index Terms*—Grazing couple remote sensing process (GCRSP) model, light use efficiency, net primary productivity (NPP), stocking rate, Zoigê wetland.**

I. Introduction

THE net primary productivity (NPP) of vegetation represents the remainder of the total amount of organic matter accumulated by green plants through photosynthesis within a unit area and unit time after deducting autotrophic respiration (Ra) [1], [2]. NPP participates in the process of the surface carbon cycle through photosynthesis [3]. The Zoigê wetland is located along the upper reaches of the Yellow River and the northeastern margin of the Tibetan Plateau [4]. In recent years, rapid economic development and global climate change have accelerated the process of grassland desertification of the Zoigê wetland, and the grassland desertification area has increased by a total of 3162.81 hm^2 from 1990 to 2013 [5]. Studies on the NPP of the grassland ecosystem of the Zoigê wetland can provide insights toward the sustainable utilization of animal and plant resources in this region and the proper distribution of regional production [6].

At present, the methods of estimating the NPP of grassland are mainly being classified into four model categories: statistical [7], light use efficiency [8], [9], process [10], and coupling [8], [11]. Statistical models rely on meteorological data and cannot simulate a growing grassland environment and its biophysical parameters; therefore, applications of these models are relatively limited. The light energy utilization model was developed in the 1990s by Potter *et al.* [9] and it uses satellite remote sensing data to invert production efficiency. Berberoglu [12] applied the Carnegie–Ames–Stanford Approach (CASA) model to invert the NPP of the mountains along the coast of the Turkish Mediterranean Sea; however, this model cannot be used directly for the regions of China, and the ecological mechanisms underlying the revealed phenomena are difficult to be explained. Physiological and ecological process models are derived by simulating the physiological processes of plants [13]. Xiao *et al.* [14] adopted the Boreal Ecosystem Productivity Simulator (BEPS) model to simulate the monthly and daily NPP of the ecosystems in North China; however, this model presented limitations associated with complicated parameters, deficient corresponding parameters, complicated physiological and ecological plant processes, and a limited understandability [15]. Eisfelder *et al.* [16] evaluated

Manuscript received May 7, 2021; revised October 1, 2021; accepted October 23, 2021. Date of publication November 4, 2021; date of current version December 30, 2021. This work was supported in part by the Independent Research Project of the State Key Laboratory of Geological Disaster Prevention (Chengdu University of Technology) and Geological Environmental Protection under Grant SKLGP2017Z005, and in part by the China Geological Survey under Grant DD20160018-04. (*Corresponding author: Zhengwei He.*)

Li He, Chengying Li, Zhengwei He, and Rui Qu are with the State Key Laboratory of Geohazard Prevention and Geoenvironment Protection, Chengdu University of Technology, Chengdu 610059, China, and also with the College of Tourism and Urban-Rural Planning, Chengdu University of Technology, Chengdu 610059, China (e-mail: heli2020@cdut.edu.cn; 15928679162@163.com; hzw@cdut.edu.cn; 406952101@qq.com).

Xian Liu is with the Department of Plant Biology, Southern Illinois University, Carbondale, IL 62901 USA (e-mail: fayeliu2017@gmail.com).

Digital Object Identifier 10.1109/JSTARS.2021.3125099

This work is licensed under a Creative Commons Attribution 4.0 License. For more information, see https://creativecommons.org/licenses/by/4.0/

and discussed the differences in the intermediate products, their impact on the calculated NPP, and the output products for the Moderate Resolution Imaging Spectroradiometer (MODIS) product-based light use efficiency model RBM and the soil-vegetation-atmosphere transport model BETHY/DLR, obtaining the BETHY/DLR calculated NPP (average annual 2010 and 2011 NPP: 136.87 and 106.69) are higher than RBM (62.14 and 54.61) and show stronger interannual variability. Guan *et al.* [18] studied the effect of altitude on the relationship between vegetation and climate in mountainous areas of Yunnan, China through NPP, and the correlation between NPP and precipitation became progressively more negative on an annual scale from positive to negative with increasing altitude. This is completely opposite to temperature. Along with the development of remote sensing and geographic information system technology, the following new method has been developed that uses remote sensing information to estimate the NPP of grassland: the coupled remote sensing process model. This model includes physiological processes and increases the reflection of spatial heterogeneity [17].

In grassland ecosystems, the influence of grazing on the yield is not negligible; therefore, in this article, we will couple the CASA model under the regional grazing condition with the BEPS model in order to develop a new grazing couple remote sensing process (GCRSP) model to estimate the regional grassland NPP. This new model takes the advantages of a process model and the light use efficiency model and fuses meteorological data, soil data, and remote sensing data. The GCRSP model has fewer complicated parameters compared with the BEPS model and presents increased spatial heterogeneity. Moreover, based on the CASA model, we will add grazing factors based on the decomposition of mixed pixels and optimize the light use efficiency data. Compared with other estimation methods that use a single model, the accuracy of the GCRSP model is higher and the algorithm is simpler. The proposed model includes physiological processes and presents more accurate regionalization capabilities.

The objectives of this article are 1) to improve the above two factors by considering the influence of livestock grazing on grassland and wetland moisture content on vegetation growth, and to propose a new GCRSP model which is suitable for the productivity of the Zoigê wetland; and 2) to analyze the area by combining field survey data with the CASA model, BEPS model, and MODIS NPP products. The accuracy of the coupled remote sensing-process GCRSP model is compared and the fit results are analyzed to determine the advantages of the GCRSP model for such regional evaluations.

II. Data and Method

A. Study Area

The Zoigê grassland is located at the northeast margin of the Tibetan Plateau, and it is under the administrative jurisdiction of Gansu and Sichuan provinces. It covers Aba County, Zoigê County, Hongyuan County of Sichuan Province, Maqu County, and Luqu County of Gansu Province (Fig. 1). The total area is 44 758 km^2. The elevation in the region is between 2392 and 5057 m, and the landform is a hilly plateau. The climate type of the study area is continental plateau cold temperate monsoon climate. The annual average temperature is approximately 0–2°C, and the annual average precipitation amount is approximately 600–700 mm. The vegetation types of Wakulgee wetland are mainly marsh vegetation and alpine meadow. Meadow vegetation is the most widely distributed vegetation, which is found in wide valleys, slopes, mountain plains, and hills. The bog vegetation is more concentrated, mainly in the middle and lower reaches of Heihe and Baihe rivers, which have poor drainage; oxbow lakes, depressions in front of mountains and wide valleys between hills and mountains.

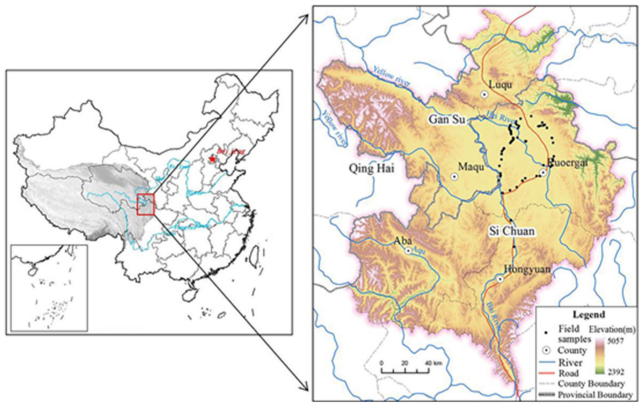

Fig. 1. Location of study area.

The field survey was carried out from July to August 2015, during the growing season of the grassland, which was largely consistent with the selected remote sensing images in terms of temporal phase. The samples were selected in areas with homogeneous and continuous vegetation types, obtained by harvesting method, and arranged in patches along the Ruoerge Nature Reserve. Based on the spatial distribution of grassland types, we selected a total of 45 sample points. The sampling points were one large sampling square (10 × 10 m) with four small representative sampling squares, and three 0.2 m × 0.2 m sampling squares were set up in the small representative areas, and all aboveground parts in the sampling squares were harvested. The weights of the preserved paper bags were determined, the bags were numbered, and the fresh grass samples were brought back to the laboratory, dried in an oven at 65°C for 48 h. The dry weight of biomass of the aboveground parts was determined using a 0.01 g sensing balance. The average dry weight of four small representative sample squares was calculated [18], with each 2.2 g of dry weight being approximately equal to 1 g of carbon [19]. These data were used to estimate the net grassland value of the sample plots.

Remote sensing data are Landsat8 images of 2015 downloaded from the official website of the United States Geological Survey.[1] The spatial resolution of the images is 30 m, and low cloud coverage is observed. Images between July and August, when the growth condition of vegetation is good, were used.

[1][Online]. Available: https://www.usgs.gov/

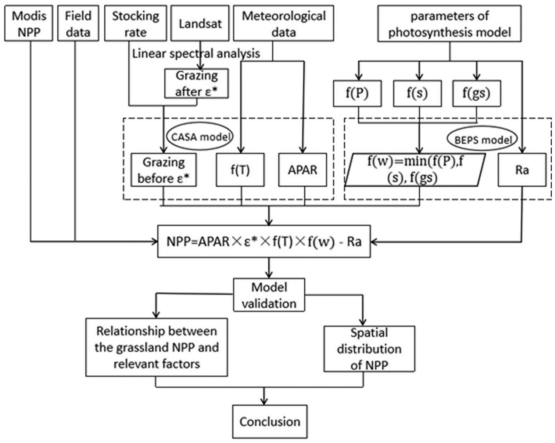

Fig. 2. Flowchart of GCRSP model.

Meteorological data, including monthly average precipitation (mm), monthly average temperature (°C), sunshine duration (h), average humidity (%), average air pressure (hPa), and total annual solar radiation (kWh/m^2) for July and August 2015, from the China National Meteorological Information Service.[2] Using ArcGIS software, we performed spatial data interpolation to process the aforementioned data to grid data with a spatial resolution of 30 m.

The grazing data in this article were acquired from the Statistical Yearbook of Aba Prefecture and Gannan Prefecture; the parameters in the photosynthesis model referred to [20], [21]; and the parameters of the Ra model referred to [22] (Fig. 1).

B. Method

The CASA model [23] is a process-based remote sensing model coupling ecosystem productivity and soil carbon and nitrogen fluxes, driven by gridded global climate, radiation, soil, and remotely sensed vegetation index datasets that require fewer parameters compared to other models. The BEPS model is a process model that combines soil, meteorological, and plant physiological parameters, and estimates vegetation NPP by simulating photosynthetic processes, with the important feature of using remotely sensed observations of leaf area index data as the main input parameter to the model [24]. In this article, we couple these two models to develop the GCRSP model (Fig. 2).

The GCRSP model simulates the gross primary productivity of vegetation (GPP), the NPP, and the consumption of Ra. In particular, NPP = GPP–Ra, and the calculation formula of Ra refers to [22]. GPP is calculated as follows:

$$\mathrm{GPP} = \mathrm{APAR} \times \varepsilon \tag{1}$$

$$\mathrm{APAR}\,(x,t) = Q\,(x,t) \times \eta \times \mathrm{FPAR}(x,t) \tag{2}$$

$$\mathrm{NPP}(x,t) = \mathrm{GPP}(x,t) - \mathrm{Ra}. \tag{3}$$

$\mathrm{GPP}(x,t)$ denotes the total primary productivity of vegetation in month *t* for the image element *x*. $\mathrm{APAR}(x,t)$ denotes the photosynthetically active radiation absorbed by image element *x* in month *t* (MJ/m^2);$Q(x,t)$ denotes the total solar radiation in month *t* (MJ/m^2);$\mathrm{FPAR}(x,t)$ indicates the proportion of absorption of incident photosynthetically effective radiation by vegetation canopy, which has a certain relationship with normalized vegetation index and specific vegetation index; and η is a constant, which indicates the proportion of solar effective radiation (wavelength of 0.38–0.71 μm) that vegetation can utilize to the total solar radiation, and is taken as 0.5.$\mathrm{NPP}(x,t)$ denotes the NPP of vegetation in month *t* for like element *x*. Ra indicates the amount of autotrophic respiration consumed.

The value of ε plays a decisive role in the process of estimating vegetation NPP [25], [26]. In this article, we improve the maximum light use efficiency and water stress factor, and achieve the optimization of ε.

C. Maximum Light Use Efficiency $\varepsilon*$

Vegetation under different environmental conditions presents different light use efficiency [27], [28]. Livestock grazing on grassland causes a loss of NPP to some extent. In the CASA model, the maximum light use efficiency for all vegetation is 0.389 gC/MJ, and the vegetation type and vegetation coverage are not differentiated, which could affect the accuracy of model calculations. The spectral mixture analysis considers the spectral characteristics of the pixel as a mixture of the spectral characteristics of different pure ground objects [29]. We incorporated a linear spectral mixture analysis into the estimation process of grassland NPP. According to the different abundances of vegetation in the pixel, we can obtain grassland NPP with different spatial distributions, thereby ensuring the accuracy of the results at the subpixel level and increasing the accuracy of NPP estimations.

Grazing has a significant influence on grassland NPP [30]. Proper grazing promotes the growth of grassland by reducing the density of grassland, which allows the vegetation to better absorb solar radiation and acquire nutrients [30], [31]. However, overgrazing affects the growth of grasslands because the compensatory growth of grasslands after grazing is less than the consumption by livestock, resulting in a reduction in the overall stock of grassland vegetation. Therefore, the influence of grazing on grassland NPP is two-sided. Remote sensing acquires imagery data after livestock grazing, and the grassland NPP estimated from these data shows varying degrees of loss. Based on the linear spectral mixture analysis, we take account of the grazing factor, obtain the vegetation abundance data of grassland prior to grazing and reduce the influence of grazing on the grassland NPP. To conveniently calculate the influence of grazing on grassland abundance, we define the stocking rate as the number of livestock per unit area of grassland in a certain period divided by the maximum carrying capacity of livestock per unit area. Therefore, the expression of grassland abundance before grazing is as follows:

$$\begin{cases} f_{gv} > 0.75 \;; F_{gv} = f_{gv} / \frac{S}{S0} \\ f_{gv} < 0.75 \;; F_{gv} = f_{gv} \times \frac{S}{S0} \end{cases} \tag{4}$$

where f_{gv} represents the vegetation abundance prior to the grazing; f_{gv} represents the vegetation abundance obtained by the inversion of remote sensing data; *S* represents the number

[2][Online]. Available: http://cdc.cma.gov.cn

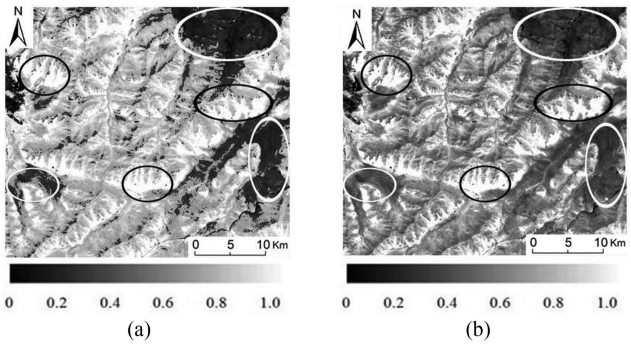

Fig. 3. Change of vegetation abundance before and after grazing. (a) Vegetation abundance after grazing. (b) Vegetation abundance before grazing. (a) Grazing Before. (b) Grazing After.

of livestock in the unit area; and S_0 represents the maximum carrying capacity of livestock in the unit area.

When $f_{gv} \geq 0.75$, the growth capacity of the grass is high, the abundance of grass before grazing is greater than after grazing, and NPP is higher than after grazing; and when $f_{gv} < 0.75$, the grassland abundance is affected by grazing. When $S > S_0$, namely, when the number of heads of livestock is higher than the maximum carrying number of heads of livestock, i.e., overgrazing occurs, grassland damage is serious, and the vegetation abundance prior to grazing is greater than the current vegetation abundance. When $S < S_0$, namely, when the number of heads of livestock is smaller than the maximum carrying number of heads of livestock, i.e., conservative grazing occurs, which can promote the growth of grassland and the vegetation abundance prior to grazing is smaller than the current vegetation abundance. Fig. 3 shows the change of vegetation abundance before and after the grazing and indicates that vegetation abundance before grazing is generally greater than the vegetation abundance after grazing. Black circle indicates the area where the vegetation abundance after grazing is smaller than the vegetation abundance prior to grazing, and white circle indicates that the area where vegetation abundance after grazing is higher than before grazing (Fig. 3).

Finally, the calculation formula for maximum light use efficiency $\varepsilon*$ is as follows:

$$\varepsilon* = F_{\mathrm{gv}} \times \varepsilon_{\max} \tag{5}$$

where f_{gv} is the grassland abundance derived by the decomposition of mixed pixels and $\varepsilon_{\max}$ is the maximum light use efficiency for grassland, and its value is 0.68 [32].

D. Water Stress Factor f(W)

Previous studies have indicated that calculation of the water stress effect coefficient involves soil moisture content, atmospheric precipitation amount, and stomatal conductance [32]–[34]. In this article, we calculated precipitation stress factor, soil moisture stress factor, and stomatal conductance stress factor separately, and then selected the values of the effects on plant growth stress.

Climate factors such as atmospheric precipitation and stomatal conductance were introduced into the model to establish a simple statistical regression model between NPP and climate factors [32], [33]. The effect of soil water stress on plant growth was calculated by soil moisture content and field water capacity. In this article, according to the calculation formula of King [35] for the soil water content, we revised the calculation formula of soil water stress factor as follows:

$$f(S) = \left(1 - b \times e^{(-c \times \mathrm{SW})}\right) / d \tag{6}$$

$$\mathrm{SW} = \frac{W_1 + W_2}{2 \times W_0} \tag{7}$$

where f(s) is the soil water stress factor, and its value is in the range of 0–1; $b = 0.86$; $c = -1.26$; $d = 0.7486$ [36]; W_1 represents the moisture content in the upper layer of soil; W_2 represents the moisture content of the lower layer of soil; and W_0 represents the field moisture capacity.

Therefore, the soil water stress factor is expressed as follows:

$$f(W) = \min(f(P), f(S), f(g_s)). \tag{8}$$

In summary, the optimized light use efficiency ε is expressed as follows:

$$\varepsilon = \varepsilon* \times f\,(T) \times f\,(W) \tag{9}$$

where $\varepsilon*$ represents the maximum light use efficiency for grassland; f(T) represents the temperature stress factor; and f(W) represents the water stress factor.

III. Results and Analysis

A. Model Validation

In previous articles, for example, Tuo *et al.* [37] utilized remote sensing process modeling to global and regional scale carbon cycle simulations, as well as forest productivity estimation [38] and crop estimation [39]. It was also applied to calculate the NPP of wetland grassland vegetation. In this article, regression analysis was used to fit the NPP data obtained from field sampling and the NPP results obtained from the GCRSP model, CASA model, and BEPS model. MODIS NPP products were then used to analyze the accuracy of the model.

After linearly fitting the measured NPP and the obtained NPP (Fig. 4) we found that the fitting between the GCRSP model and measured NPP was the best with $R_2 = 0.84$. The correlation coefficient between the CASA model and the measured NPP fit was 0.61. Comparison results proved that the actual modeling effect obtained using a single CASA model was not accurate, as pointed out in the study by Jin *et al.* [33]. A more detailed modification of the major species in the biological community would help improve modeling accuracy. The BEPS model had the worst fit to the measured NPP with $R_2 = 0.51$, indicating that the GCRSP model inversion was more accurate. The GCRSP model was fitted to the MODIS NPP product with $R_2 = 0.11$, which was poorly correlated (Fig. 4).

B. Spatial Distribution of NPP in Zoigê Wetland and Analysis of Model Calculation Results

A comparison of the grassland NPP obtained by the three methods and the MODIS NPP products (Fig. 5) showed that the

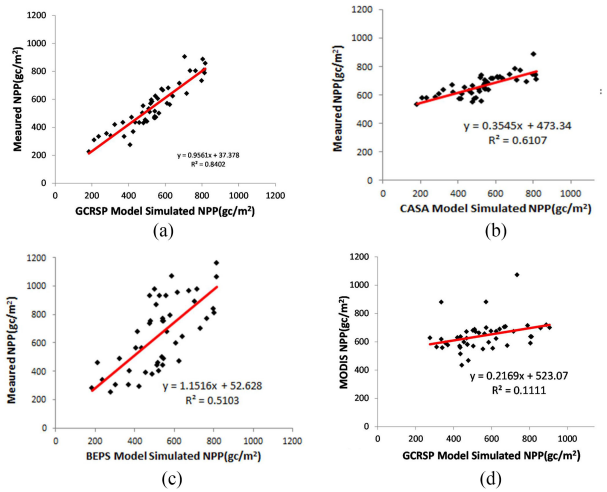

Fig. 4. Linear fittings between the measured NPP of the sample sites and the obtained NPP. (a) Relationship between the NPP from the GCRSP model and the measured NPP. (b) Relationship between the NPP from the CASA model and the measured NPP. (c) Relationship between the NPP from the BEPS process model and the measured NPP. (d) Relationship between the GCRSP model and the MODIS NPP data. (a) GCRSP Model Simulated NPP(gc/m^2). (b) CASA Model Simulated NPP(gc/m^2). (c) BEPS Model Simulated NPP(gc/m^2). (d) GCRSP Model Simulated NPP(gc/m^2).

TABLE I
NPP RESULTS OF THE ZOIGÊ WETLAND OBTAINED BY THE THREE MODELS

County	GCRSP model		CASA model		BEPS process model	
	Maximum NPP (gC/m^2)	Mean NPP (gC/m^2)	Maximum NPP (gC/m^2)	Mean NPP (gC/m^2)	Maximum NPP (gC/m^2)	Mean NPP (gC/m^2)
Zoigê County	1401	606.60	1135	500.31	1517	611.39
Aba county	1390	649.32	1079	514.48	1497	711.78
Hongyuan County	1351	597.74	1113	494.93	1433	569.42
Maqu County	1387	576.27	1027	471.56	1462	607.51
Luqu County	1092	515.17	924	414.73	1298	567.85
Entire research area	1401	586.39	1135	487.57	1631	620.95

spatial distribution was generally consistent at the macroscopic level [40]. Grassland NPP was low in the range of 0–200 gC/m^2 in the vicinity of alpine glaciers and around wetlands, where low temperature and land desertification were the greatest dragging factors. Grassland NPP values were greater along rivers and in wetland vegetation growth areas, which is in agreement with [41]. A spatial distribution pattern of NPP can be observed, where the distribution of grasslands at 3400–3500 m elevation accounted for 78% of the total grassland area and 58% of the total grassland with slopes less than 1°. It showed that the spatial distribution pattern of NPP was highly correlated with topographic factors, and NPP was high in the Heihe River mainstream terrace, an area with rich herbaceous peat swamp soil and high NPP of grasslands.

The NPP values obtained by the three models exhibited macroscopic similarities, although differences were observed

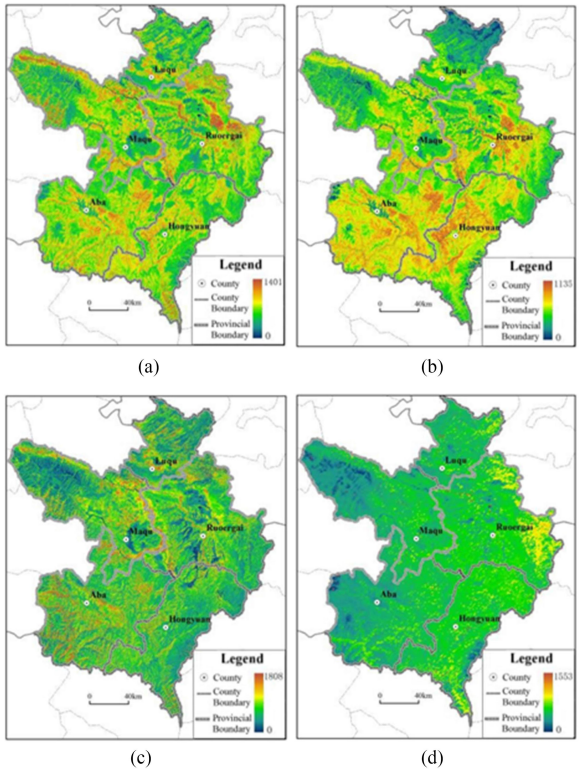

Fig. 5. NPP spatial distribution obtained by the three models. (a) Spatial distribution of NPP obtained by the GCRSP model. (b) Spatial distribution of NPP obtained by the traditional CASA model. (c) Spatial distribution of NPP obtained by the BEPS process model. (d) MODIS NPP product.

in the distribution of values (Table I). The statistical results for the entire research area indicated that the NPP values obtained by the traditional CASA model were relatively small and had a maximum of 1135 gC/m^2 and mean of 487.57 gC/m^2. NPP values obtained by the BEPS process model were relatively large and had a maximum of 1808 gC/m^2 and mean of 620.95 gC/m^2, and these values are generally relatively scattered, thus showing an obvious contrast. In contrast, the GCRSP model yielded relatively uniform NPP values, with a maximum of 1401 gC/m^2 and an average of 586.39 gC/m^2, indicating that the results of the GCRSP model were all within a reasonable range (Fig. 5).

The difference values between BESP and GCRSP models were mainly concentrated between 0% and 27% with a mean value of 17.48%. The difference values between CASA and GCRSP models are mainly concentrated between 5% and 39%, with a mean value of 24.74% (Fig. 6).

C. Relationship Between the Stocking Rate and Grassland NPP

With reference to Hugejiletu Jin *et al.*'s study on NPP prediction in the Mongolian plateau, changes in NPP in the plateau can be affected by natural conditions such as grazing [30], and the inclusion of factors such as regional grazing practices which can increase the reliability of the model. Therefore, the analysis of the relationship between grazing rate and NPP can provide important value for the calculation of grassland NPP. In this article, we took account of the differences in NPP before and

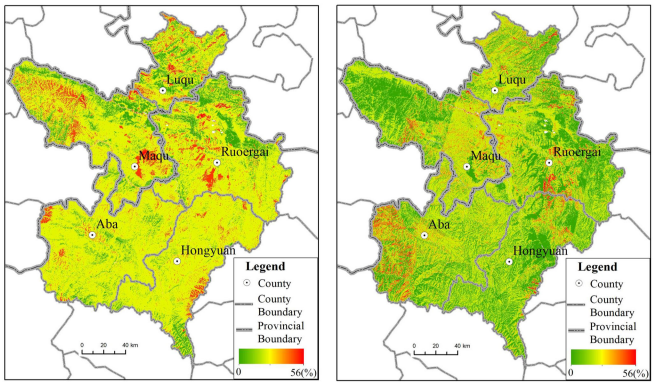

Fig. 6. NPP results comparison difference chart. (a) CASA and GCRSP models. (b) BESP and GCRSP models.

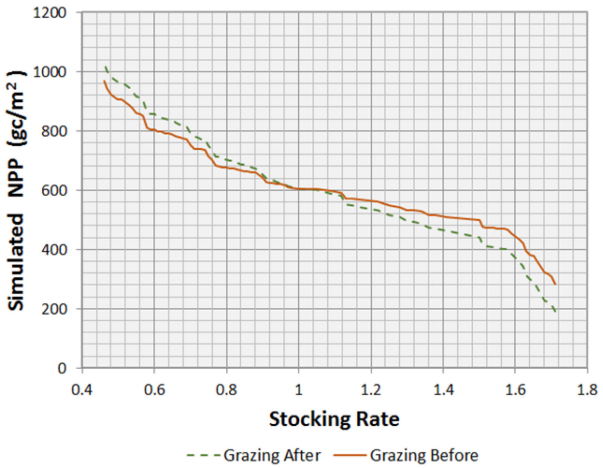

Fig. 7. Relationship between grassland NPP and stocking rate before and after the grazing.

after grazing in Jorge wetland (Fig. 7). When the grazing rate was less than 1, the NPP after grazing was slightly larger than before grazing; when the grazing rate was greater than 1, the NPP after grazing was significantly smaller than before grazing; and when the grazing rate was greater than 1.46, the rate of decline of grassland NPP was faster.

D. Relationship Between the Grassland NPP and Relevant Factors

Relationship between grassland NPP and temperature [Fig. 8(a)]. In general, as the temperature increased, the NPP value gradually increased. Within the range of 11°C –13.5°C, NPP increased at a relatively fast rate with the increasing temperature, whereas in the range of 13.5°C –17°C, temperature for grassland growth reached its optimal value, and the NPP value tended to be stable afterwards.

Relationship between grassland NPP and precipitation [Fig. 8(b)]. As the precipitation increased, the NPP value for the Zoigê wetland gradually increased. A relatively strong linear relationship was observed between the precipitation and NPP. The increased precipitation provided sufficient water for grassland

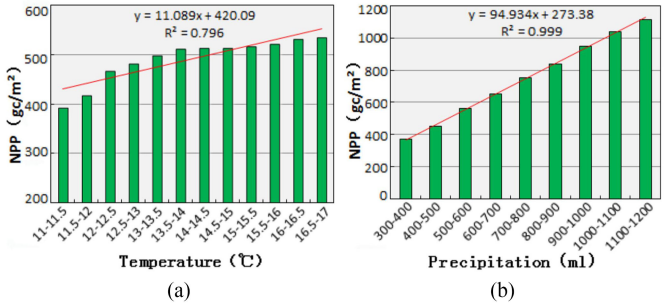

Fig. 8. Influence of meteorological factors on the grassland NPP of the Zoigê wetland. (a) Relationship between the mean NPP and temperature. (b) Relationship between the mean NPP and precipitation.

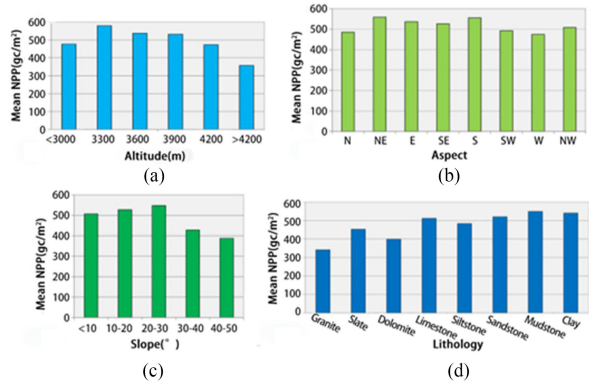

Fig. 9. Influence of topographical factors on the grassland NPP of the Zoigê grassland. (a) Relationship between the mean NPP and elevation. (b) Relationship between the mean NPP and azimuth angle. (c) Relationship between the mean NPP and slope. (d) Relationship between the mean NPP and lithology.

growth, and the maximum NPP was reached at a precipitation level of approximately 1200 ml.

Relationship between the grassland NPP and elevation [Fig. 9(a)]. As the elevation increased, the NPP value initially increased and then decreased. The solar radiation received by vegetation is strengthened with increasing elevation, which leads to increased NPP. At elevations in the range of 3300–3900 m, the maximum grassland NPP is observed. With further increases in elevation, both temperature and NPP value declined.

Relationship between grassland NPP and azimuth angle [Fig. 9(b)]. The relationship between the grassland NPP and azimuth angle was statistically analyzed in a clockwise direction starting from the north. The grassland NPP was largest in the northeast, east, southeast, and south. The study area was in the north of the Tropic of Cancer, and sunlight irradiates from the south. Grassland receives more solar radiation in this direction, and the grassland NPP is relatively small in the other directions.

Relationship between grassland NPP and slope [Fig. 9(c)]. As the slope increased, the grassland NPP initially increased and then decreased, with the maximum value observed in the range of 20°–30°. This range provides the optimal reception of solar radiation by grassland, which is not only favorable for water storage but also for drainage. This finding is consistent with previous studies, such as Gao *et al.* [6], who studied grassland NPP in northern Tibet and concluded that when the slope is in the range of 20°–25°, the maximum NPP is observed; and Zhao

[45], who performed a simulation study on the vegetation NPP of Qinghai and concluded that the maximum NPP is reached when the slope is in the range of 10°–15°. The results of the current article are essentially consistent with these previous conclusions.

Relationship between grassland NPP and lithology [Fig. 9(d)]. The NPP value varies for different lithologies. Granite belongs to acidic magmatic rocks, and vegetation cannot survive on these rocks; therefore, the grassland NPP values for regions with a granite lithology are relatively low. Slate is a metamorphic rock and thus it is fragile and prone to be weathered. Vegetation can develop on these rocks, and the grassland NPP values for regions with a slate lithology are relatively high compared with regions with a granite lithology. Dolomite, limestone, siltstone, sandstone, and mudstone are sedimentary rocks, which contain organic matter and present a relatively high number of pores and fissures, and thus they are easy to be weathered. Vegetation can develop on these, and the grassland NPP value is relatively high in regions with such lithologies. The NPP of mudstone is the largest. Clay originates from alluvium and diluvium in the Holocene, and it is rich in organic matter and is suitable for plant growth. Thus, the NPP value for regions with a clay lithology is relatively large.

IV. Conclusion

This article couples the CASA model with the BEPS model based on regional grazing conditions, while integrating the relationship between the concept of grazing rate and NPP to provide an effective reference for the calculation of grassland NPP, and the main conclusions are as follows.

Comparing the grassland NPP and MODIS NPP products obtained from the three models, the spatial distribution of the NPP is basically consistent at the macro level. Grassland NPP is lower in the vicinity of alpine glaciers and wetlands, and the low temperature and land desertification are the biggest dragging factors in this area; the grassland NPP is larger along rivers and wetland vegetation growth areas, where herbaceous peat bog soils are abundant. From the statistical results of the whole study area, the value of NPP obtained by the traditional CASA model was small, with a mean value of 487.57 gC/m^2, which was more concentrated overall. The value of NPP obtained by the BEPS process model was larger, with a mean value of 620.95 gC/m^2, which was more scattered overall and the contrast was obvious. The NPP obtained by the GCRSP model was more homogeneous, with a mean value of 586.39 gC/m^2. By comparing the suitability of the results, the GCRSP model yielded more accurate results than the other two methods.

In this article, a new GCRSP model for estimating regional grassland NPP was developed by coupling the CASA model and BEPS model under grazing conditions. Remote sensing process coupling model will be a major development direction for wetland vegetation NPP estimation. In the analysis of the actual linear fit relationship of the GCRSP model, it was found that the GCRSP model had the best fit with the measured NPP, $R_2 = 0.84$; it integrated the advantages of both the process model and the light energy utilization model. It not only realized the compatibility of multisource data (including remote sensing data, meteorological data, ground sampling data, etc.), but also mechanistically explained the plant growth and development mechanism, with clearer physical significance. A new tool for estimating wetland vegetation NPP is provided.

References

[1] Z. Chi, W. Shaohong, and L. Guoyong, "Possible changes in the NPP of China's terrestrial ecosystems and identification of risk areas in the 21st century: Based on the BCC-CSM2 model," *J. Geogr. Sci.*, vol. 30, no. 8, pp. 1219–1232, 2020.

[2] Q. Huang, W. Ju, F. Zhang, and Q. Zhang, "Roles of climate change and increasing CO_2 in driving changes of net primary productivity in China simulated using a dynamic global vegetation model," *Sustainability*, vol. 11, no. 15, 2019, Art. no. 4176.

[3] B. Li and R. Zhiyuan, "Estimation and trend analysis of net primary productivity in Yinchuan basin," *China Agricultural Sci.*, vol. 49, no. 7, pp. 1303–1314, 2016.

[4] Z. Lian, Z. Wenxiu, L. Gang, C. Qin, D. Ligang, and H. Zhengjun, "Evaluation of the service value of main ecosystems in Zoige County: Taking the degraded grassland improvement demonstration project area in Zoige as an example," *Grass Ind. Animal Husbandry*, vol. 38, no. 1, pp. 48–51, 2013.

[5] L. Yu, *Analysis of the Temporal and Spatial Changes of Desertified Grassland in Zoige Wetland Reserve Based on Remote Sensing*. Ya'an, China: Sichuan Agricultural Univ., 2014.

[6] Q. Z. Gao, Y. F. Wan, Y. E. Li, W. P. Sheng, and W. F. Li, "Trends of grassland NPP and its response to human activity in northern Tibet," *Acta Ecologica Sinica*, vol. 27, no. 11, pp. 4612–4619, 2007.

[7] W. Jiyan, L. Ainong, and J. Hua'an, "A review of wetland vegetation net primary productivity estimation models," *Wetland Sci.*, vol. 13, no. 05, pp. 636–644, 2015.

[8] Z. Ping, W. Wei, W. Rui, L. Tao, and S. Chengming, "Simulation and computational analysis of different grassland NPP estimation models for Chinese grasslands," *Grassland Sci.*, vol. 35, no. 10, pp. 2381–2388, 2018.

[9] C. S. Potter *et al.*, "Terrestrial ecosystem production: A process model based on global satellite and surface data," *Global Biogeochem. Cycles*, vol. 7, no. 4, pp. 811–841, 1993.

[10] Q. Sun *et al.*, "An improved biome-BGC model for estimating net primary productivity of alpine meadow on the Qinghai-Tibet plateau," *Ecol. Modelling*, vol. 350, pp. 55–68, 2017.

[11] W. Junbang, L. Jiyuan, S. Quanqin, L. Ronggao, F. Jiangwen, and C. Zhuoqi, "Simulation of net primary productivity in the source region of the three rivers in Qinghai from 1988 to 2004 based on a remote sensing-process coupling model," *Chin. J. Plant Ecol.*, vol. no. 33, no. 2, pp. 23–38, 2009.

[12] H. Su, B. E. Fatih, O. Coskun, and D. Cenk, "Modeling forest productivity using Envisat MERIS data," *Sensors*, vol. 7, no. 10, pp. 2115–2127, 2007.

[13] C. Wen, "Model methods and mechanisms of vegetation NPP estimation," in *Proc. Anhui Agricultural ENCE Bull.*, 2014, Art. no. 965936.

[14] M. Xiao, Z. L. Guang, M. Colton, and A. Ernesto, "Combining multi-source remotely sensed data and a process-based model for forest above-ground biomass updating," *Sensors*, vol. 17, no. 9, 2017, Art. no. 2062.

[15] C. Yi-Zhao, L. I. Jian-Long, S. Zheng-Guo, and G. Cheng-Cheng, "Spatio-temporal dynamics of grassland net primary productivity and its response to climate change in the temperate Eurasian steppe 1982–2008," *Acta Prataculturae Sinica*, vol. 26, no. 1, pp. 1–12, 2017.

[16] C. Eisfelder, C. Kuenzer, and S. Dech, "Derivation of biomass information for semi-arid areas using remote-sensing data," *International Journal of Remote Sensing*, vol. 33, no. 9, pp. 2937–2984, 2012, doi: 10.1080/01431161.2011.620034.

[17] C. Eisfelder, C. Kuenzer, S. Dech, and M. F. Buchroithner, "Comparison of two remote sensing based models for regional net primary productivity Estimation—A case study in semi-arid central Kazakhstan," *IEEE J. Sel. Topics Appl. Earth Observ. Remote Sens.*, vol. 6, no. 4, pp. 1843–1856, Aug. 2013.

[18] X. Guan, H. Shen, X. Li, W. Gan, and L. Zhang, "Climate control on net primary productivity in the complicated mountainous area: A case study of Yunnan, China," *IEEE J. Sel. Topics Appl. Earth Observ. Remote Sens.*, vol. 11, no. 12, pp. 4637–4648, Dec. 2018.

[19] S. Liu, Q. Shi, and L. Zhang, "Few-shot hyperspectral image classification with unknown classes using multitask deep learning," *IEEE Trans. Geosci. Remote Sens.*, vol. 59, no. 6, pp. 5085–5102, Jun. 2021.

[20] Q. Shi, X. Tang, T. Yang, R. Liu, and L. Zhang, "Hyperspectral image denoising using a 3-D attention denoising network," *IEEE Trans. Geosci. Remote Sens.*, vol. 59, no. 12, pp. 10348–10363, Dec. 2021.

[21] L. Chang, J. Guangchao, C. Changchun, W. Shenmin, Y. Xuhong, and X. Xiaomin, "Overview on estimation models of land net primary productivity integrating remote sensing data," *Prog. Geogr.*, vol. 36, no. 8, pp. 924–939, 2017.
[22] L. Chengxiu, C. Guangchao, W. Chengyong, and C. Kelong, "Study on NPP remote sensing estimation model based on data of landsat8 OLI in mountainous area," *J. Green Sci. Technol.*, vol. 31, no. 5, pp. 875–885, 2016.
[23] S. L. Piao, J. Y. Fang, J. S. He, and Y. Xiao, "Spatial distribution of grassland biomass in China," *Acta Phytoecologica Sinica*, vol. 28, no. 4, pp. 491–498, 2004.
[24] J. M. Chen, J. Liu, J. Cihlar, and M. L. Goulden, "Daily canopy photosynthesis model through temporal and spatial scaling for remote sensing applications," *Ecol. Modelling*, vol. 124, no. 2–3, pp. 99–119, 1999.
[25] X. Jing, C. Di, L. Wenlong, and W. Wei, "Study on the net primary productivity of vegetation in Gannan prefecture based on the model of light energy utilization efficiency," *Pratacultural Sci.*, vol. 36, pp. 2455–2465, 2019.
[26] D. L. Seen, E. Mougin, S. Rambal, A. Gaston, and P. Hiernaux, "A regional sahelian grassland model to be coupled with multispectral satellite data II. Toward the control of its simulations by remotely sensed indices," *Remote Sens. Environ.*, vol. 52, no. 3, pp. 194–206, 2011.
[27] G. Bao *et al.*, "Modeling net primary productivity of terrestrial ecosystems in the semi-arid climate of the Mongolian plateau using LSWI-based CASA ecosystem model," *Int. J. Appl. Earth Observ. Geoinf.*, vol. 46, pp. 84–93, 2016.
[28] A. Govind, J. M. Chen, H. Margolis, W. Ju, O. Sonnentag, and M.-A. Giasson, "A spatially explicit hydro-ecological modeling framework (BEPS-TerrainLab V2.0): Model description and test in a Boreal ecosystem in eastern North America," *J. Hydrol.*, vol. 367, no. 3/4, pp. 200–216, 2009.
[29] S. Xuemei, *Research on the Inversion of Light Energy Utilization in Meadow Steppe*, Hohhot, China: Inner Mongolia Normal Univ., 2013.
[30] X. Ya and W. W. Liwen, "The study on simulating light use efficiency of vegetation in Qinghai Province," *Acta Ecologica Sinica*, vol. 30, pp. 5209–5216, 2010.
[31] P. Shaolin, G. Zhihua, and W. Boxun, "Using GIS and RS to estimate the light efficiency of vegetation in Guangdong," *Acta Ecologica Sinica*, vol. 20, no. 6, pp. 903–909, 2000.
[32] G. P. Asner and K. B. Heidebrecht, "Desertification alters regional ecosystem–climate interactions," *Global Change Biol.*, vol. 11, no. 1, pp. 182–194, 2010.
[33] H. Jin *et al.*, "Modifying the maximal light-use efficiency for enhancing predictions of vegetation net primary productivity on the Mongolian plateau," *Int. J. Remote Sens.*, vol. 41, no. 10, pp. 3740–3760, 2020.
[34] W. Yanfen and W. Shiping, "The effect of different grazing rates on the stock and net primary productivity and quality of the typical grasslands in inner Mongolia," *Acta Prataculturae Sinica*, vol. 10, no. 7, pp. 3–5, 1999.
[35] Z. Meiling, *Improved CASA Model Based on Grassland Comprehensive Sequential Classification System and its Application in NPP Estimation of Grassland in China*, Gansu, China: Gansu Agricultural Univ., 2012.
[36] W. Junbang, *Research on the Remote Sensing Model of China's Terrestrial Net Ecosystem Productivity*. Hangzhou, China: Zhejiang Univ., 2004.
[37] C. Tuo, F. Hu-Yuan, X. U. Shi-Jian, Q. Wei-Ya, and A. N. Li-Zhe, "Stable carbon isotope composition of desert plant leaves and water-use efficiency," *J. Desert Res.*, vol. 22, no. 3, pp. 288–291, 2002.
[38] Z. Ning-Ning, "Accuracy analysis and improvement of BIOME3 model used in China," *Climatic Environ. Res.*, vol. 13, pp. 21–30, 2008.
[39] D. A. King, D. P. Turner, and W. D. Ritts, "Parameterization of a diagnostic carbon cycle model for continental scale application," *Remote Sens. Environ.*, vol. 115, no. 7, pp. 1653–1664, 2011.
[40] D. P. Turner *et al.*, "A diagnostic carbon flux model to monitor the effects of disturbance and interannual variation in climate on regional NEP," *Tellus B*, vol. 58, no. 5, pp. 476–490, 2006.
[41] J. M. Chen *et al.*, "Effects of foliage clumping on the estimation of global terrestrial gross primary productivity," *Global Biogeochem. Cycles*, vol. 26, no. 1, 2012, Art. no. 51796197.
[42] S. Wang, L. Zhou, J. Chen, W. Ju, X. Feng, and W. Wu, "Relationships between net primary productivity and stand age for several forest types and their influence on China's carbon balance," *J. Environ. Manage.*, vol. 92, no. 6, pp. 1651–1662, 2011.
[43] J. Huaan, W. Jindi, B. Yanchen, C. Guifen, and X. Huazhu, "Regional corn yield estimation based on crop growth model and remote sensing data assimilation," *Trans. Chin. Soc. Agricultural Eng.*, vol. 28, pp. 162–173, 2012.
[44] J. Bian, A. Li, and W. Deng, "Estimation and analysis of net primary productivity of Zoigê wetland in China for the recent 10 years based on remote sensing," *Procedia Environ. Sci.*, vol. 2, pp. 288–301, 2010.
[45] Z. Guoshuai, *A Simulation Study on the Net Primary Productivity of Qinghai Vegetation Based on the Light Energy Utilization Model*. Harbin, China: Northeast Forestry Univ., 2011.

Li He received the B.S. degree in geology from the Chengdu University of Technology, Chengdu, China, in 2014, and the direct Ph.D. degree in physical geography from the Chengdu Institute of Mountain Hazards and Environment, China, in 2020.

She is currently a Lecturer with the College of Tourism and Urban-Rural Planning, Chengdu University of Technology, Chengdu, China. Her research interests include remote sensing of resources and environment.

Chengying Li received the B.S. degree in geographic information science and the M.S. degree in cartography and geographic information system from Chengdu University of Technology, Chengdu, China, in 2016 and 2020, respectively.

Zhengwei He received the B.S. and M.S. degrees in geology from Jilin University, Jilin, China, in 1989 and 1992, respectively, and the Ph.D. degree in geology from the Chengdu University of Technology, Chengdu, China, in 1998.

He is currently a Professor with the College of Geophysics, Chengdu University of Technology, Chengdu, China. His research interests include remote sensing of resources and environment, metallogenic regularity and metallogenic prediction, geographic information system, and ecological environment evaluation.

Xian Liu received the Ph.D. degree in environmental studies from Southern Illinois University, Carbondale, IL, USA, in 2021.

She is currently with the Center for Ecology, Southern Illinois University Carbondale. Her research interests include modeling non-native invasive plant species distributions in Southern Illinois under climate change.

Rui Qu received the M.S. degree in environmental studies from Chengdu University of Technology, Chengdu, China, in 2019, where he is currently working toward the Ph.D. degree in geological resources and geological engineering.

His research interests include quaternary geology and remote sensing of resources and environment.